

Calibration study of the X - T relation for the BESIII drift chamber^{*}

KANG Xiao-Lin(康晓琳)^{1,2;1)} WU Ling-Hui(伍灵慧)^{1;2)} WU Zhi(吴智)¹⁾ LUO Tao(罗涛)³⁾
 HU Chen(胡琛)⁴⁾ WANG Hai-Xia(王海霞)⁵⁾ FANG Shuang-Shi(房双世)¹⁾ HE Kang-Lin(何康林)¹⁾
 LI Wei-Dong(李卫东)¹⁾ LI Wei-Guo(李卫国)¹⁾ LIU Huai-Min(刘怀民)¹⁾ MAO Ze-Pu(毛泽普)¹⁾
 WANG Liang-Liang(王亮亮)¹⁾ YUAN Ye(袁野)¹⁾ ZHANG Yao(张瑶)¹⁾

¹⁾ Institute of High Energy Physics, Chinese Academy of Sciences, Beijing 100049, China

²⁾ University of Chinese Academy of Sciences, Beijing 100049, China

³⁾ University of Hawaii, Honolulu, Hawaii 96822, USA

⁴⁾ Nanjing Normal University, Nanjing 210023, China

⁵⁾ Central China Normal University, Wuhan 430079, China

Abstract: Offline calibration plays an important role in BESIII offline data processing. In order to achieve good spatial and momentum resolution, it is necessary to implement high precision offline calibration for the BESIII drift chamber. This paper studies the time-to-distance relations, which are important calibration constants for track reconstruction. The parameterization of the time-to-distance relation, studies of left-right asymmetry and studies of variation with entrance angle are performed. The impact of dead channels on the time-to-distance relation is given special attention in order to reduce the shift in measured momentum for tracks passing near dead cells. Finally we present the resolutions for barrel Bhabha events ($|\cos\theta| < 0.8$) from a J/ψ data set taken in 2012. The average spatial resolution is 123 μm and the momentum resolution for 1.548 GeV/ c Bhabha tracks is 11.9 MeV/ c .

Key words: BESIII, drift chamber, X - T relation, calibration

PACS: 29.40.Cs, 29.40.Gx, 06.20.fb **DOI:** 10.1088/1674-1137/39/2/026002

1 Introduction

The Beijing Spectrometer III (BESIII) [1], which operates at the upgraded Beijing Electron-Positron Collider (BEPC II) [2], aims at precision measurements and new physics searches in the τ -charm energy region. The central tracking system of BESIII is a cylindrical multi-layered drift chamber with 24 stereo layers and 19 axial layers in total. A helium-based gas mixture of He/ C_3H_8 (60/40) was chosen to minimize the effect of multiple scattering. The BESIII drift chamber operates in a 1 T magnetic field and is required to provide good spatial resolution (130 μm) and good momentum resolution (0.5%@1 GeV/ c).

In order to meet these requirements, precise offline tracking calibration and alignment are essential. The offline calibration software for the drift chamber, which is developed in the BESIII Offline Software System [3], contains the calibration of the time-to-distance relation (X - T relation), time offset (T_0) and time walk effects (Q - T relation). Time offset, which is determined cell by cell, is corrected by the difference between the measured and es-

timated drift distance [4, 5]. The calibration of time walk effects is determined from the time shift as a function of ADC output (Q) for each layer [4]. The calibration of the X - T relations is more complicated than those of time offset and time walk effects. We use different X - T relations for different layers to account for the variations in cell size and electric field. In order to achieve good spatial resolution, we also take into account the left-right asymmetry, the dependence on the incident direction of the track and other factors such as dead channels.

In this paper we introduce how the X - T relation is parameterized, describe studies of the above-mentioned issues that affect X - T relations and give the present resolutions of the drift chamber using a J/ψ data set that was collected in 2012. The Bhabha events we used are detected in the barrel region of the detector ($|\cos\theta| < 0.8$).

2 Cell geometry and the parameterization of the X - T relation

The drift cell of the BESIII drift chamber has an al-

Received 12 May 2014, Revised 28 June 2014

^{*} Supported by National Natural Science Foundation of China (11205184, 11205182, 11121092, 11179020) and Joint Funds of National Natural Science Foundation of China (U1232201)

1) E-mail: kangxl@mail.ihep.ac.cn

2) E-mail: wulh@mail.ihep.ac.cn

©2015 Chinese Physical Society and the Institute of High Energy Physics of the Chinese Academy of Sciences and the Institute of Modern Physics of the Chinese Academy of Sciences and IOP Publishing Ltd

most square trapezoidal shape. A total of 6796 cells are arranged in 43 cylindrical layers. Each sense wire is surrounded by eight field wires. The cell size is approximately $12\text{ mm}\times 12\text{ mm}$ for the inner 8 layers and $16.2\text{ mm}\times 16.2\text{ mm}$ for the others. The sense wires are connected to high voltage cables via an insulating feedthrough and all of the field wires are kept at ground.

The X - T relation is affected by the gas mixture, and by the electric and magnetic fields. A typical scatter plot of the drift distance as a function of drift time, obtained using fitted tracks from BESIII events, is shown in Fig. 1. The X - T relation is smooth over most of the cell's extent. In the region near the cell edge, winding drift lines result in long drift times. The parameterization of the X - T relation is the first step in the calibration procedure. In the Belle experiment, the X - T relation of the central drift chamber (CDC) is fitted with up to fifth-order polynomials [6]; the KLOE drift chamber uses up to fifth-order Chebychev polynomials [7].

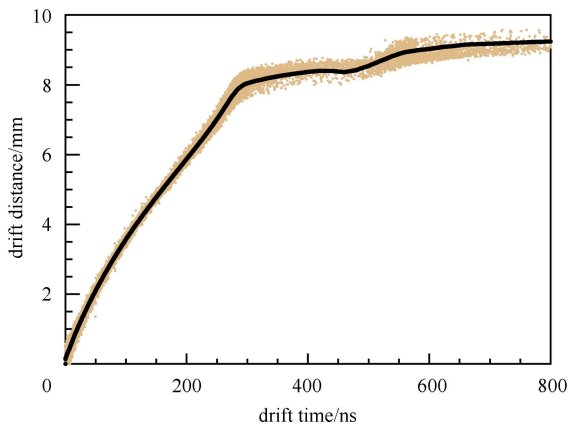


Fig. 1. Typical X - T relationship for BESIII drift chamber. The scattered points are predicted from track fitting and the black line is obtained from calibration.

Since the BESIII chamber has a similar cell geometry to that of the Belle CDC, we tried to use the same fitting function. However, this does not fit the region near the cell edge very well. Instead we use a numerical method rather than an analytical expression, similar to the procedure used by the CLEO III drift chamber group¹⁾. A time-to-distance table is saved in a calibration file and an interpolation procedure is used in the reconstruction. In Fig. 1, the scattered points are obtained from track fitting while the black line is the result of calibration, and they fit very well. Fig. 2 presents the mean value of residual distribution as a function of drift time. The shift shown in the figure is very small compared with the spatial resolution, so it can safely be neglected.

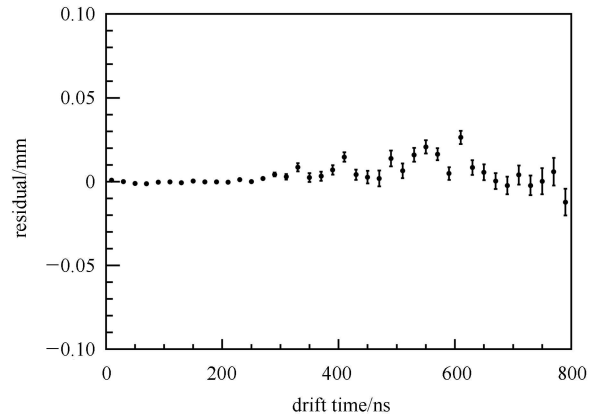


Fig. 2. The mean value of residual distribution versus drift time.

3 Left-right asymmetry

The trapezoidal shape of the cell in the cylindrical drift chamber can cause a radial electric field asymmetry. For cells in non-boundary layers, the asymmetry is small and has been further reduced by optimizing the space between the sense and field layers [8]. But for cells in boundary layers (including axial-stereo boundaries), a large asymmetry in the radial electric field can lead to a big difference between the left- and right-side X - T relations [9]. Although a compensating 100–300 V potential on the boundary field wires would effectively minimize this asymmetry [10], this was not applied in order to avoid the reduction of anti-noise capabilities. We therefore calibrated the X - T relations for the left and right sides separately. Fig. 3 shows the difference between the left and right drift distance as a function of drift time for cells in boundary and non-boundary layers. The left-right asymmetry for cells in boundary layers can be as high as 0.4 mm.

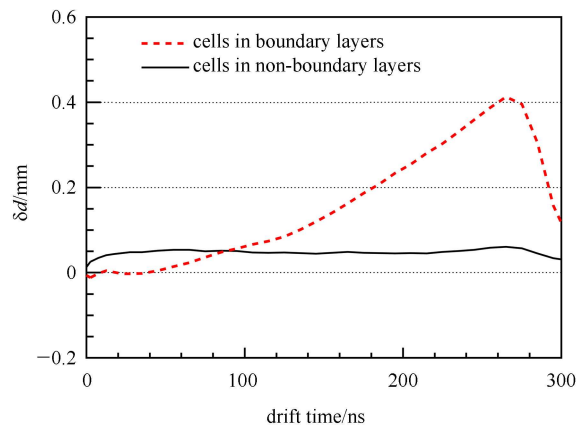


Fig. 3. Left-right asymmetry of the X - T relations. δd is the difference between the left and right drift distance.

1) Dan Peterson. Private communication.

4 Variation of the X - T relation with entrance angle

In trapezoidal-shaped drift cells, the X - T relationship depends on the incident direction of the track, i.e. on the entrance angle α , which is defined as the difference in azimuth angle between the track (the direction tangent to the hit) and the direction from the origin point to the wire in the r - ϕ plane, i.e. $\phi_{\text{track}} - \phi_{\text{wire}}$. The full domain of α , which depends on the transverse momentum of the track, is $[-\pi/2, \pi/2]$. Fig. 4 shows the predicted α in each layer based on fitted ideal helices for tracks of different momenta which pass through the origin. For a given track, $|\alpha|$ increases with the layer radius. Within the same layer, $|\alpha|$ varies inversely with the transverse momentum.

Bhabha and dimuon samples, which consist of high momentum tracks, are usually used in calibration. If we use X - T relations calibrated only from these samples on physical events which contain a lot of low momentum tracks, a bias is unavoidable. The bias can be found

in residual distributions, as shown in Fig. 5(a). These residual shifts can be as high as 0.15 mm for regions far from the sense wires.

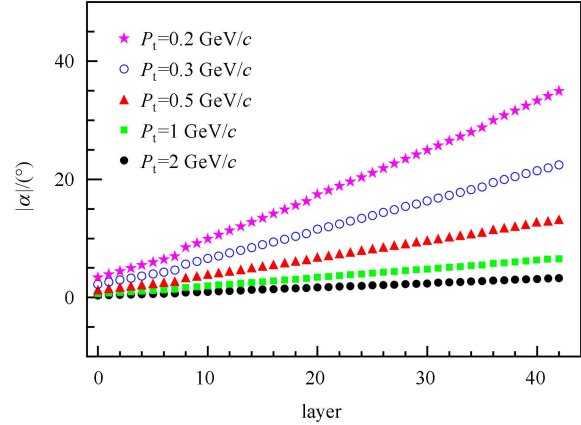


Fig. 4. Entrance angles in different layers for tracks of different momenta.

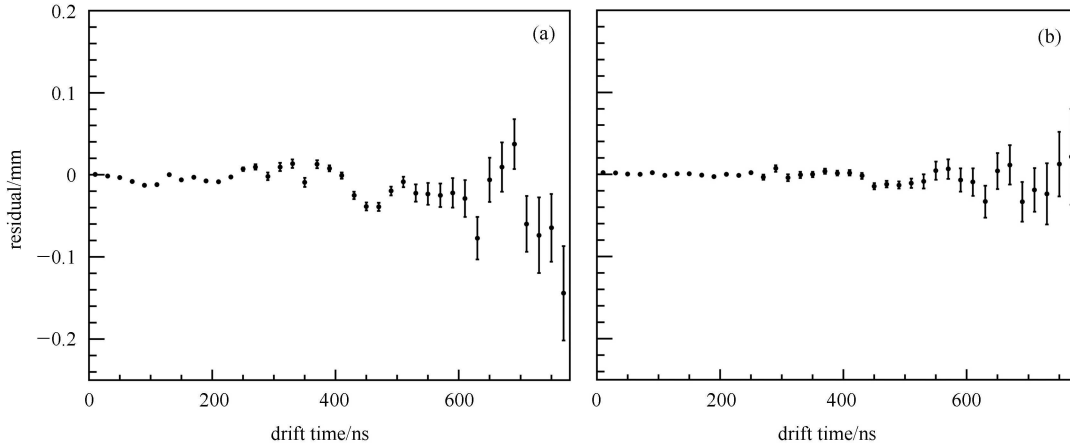


Fig. 5. The mean value of residual distribution as a function of drift time for P_t less than 0.5 GeV/c, (a) using X - T relations calibrated from Bhabha samples; and (b) using X - T relations calibrated from π and Bhabha samples.

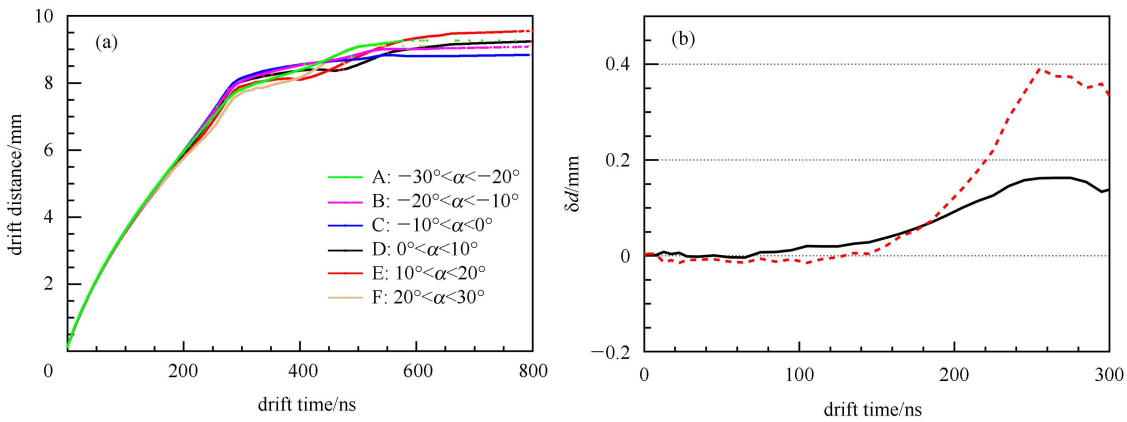


Fig. 6. (a) X - T relations for different entrance angles in layer 30; (b) the difference in drift distance between E and D (solid line), F and D (dashed line), as a function of drift time.

This makes it necessary to combine both low momentum and Bhabha track samples in the calibration procedure. For example, for the J/ψ data set, we choose π tracks from $J/\psi \rightarrow \rho\pi$ where the purity of the pion is 99.9%. Separate X - T relations are determined for different entrance angles, with a step size of 10 degrees. Fig. 5(b) shows the mean value of the residual distribution as a function of drift time after calibration, and it is clear that the bias is much smaller than in Fig. 5(a). Figure 6(a) shows the X - T relations for different entrance angles in layer 30. Fig. 6(b) shows the differences in X - T relations between two sets of adjacent α steps. It is evident that the differences are very small near the sense wires, but grow up to several hundred microns with increasing drift times.

5 Impact of dead channels on the X - T relation

Unavoidably, the BESIII drift chamber will develop some dead channels during data taking periods, which are usually caused by bad preamplifier cards. Each preamplifier card covers eight channels. For example, during collection of the 2012 J/ψ data set, a bad preamplifier caused 8 dead channels (cells 161 to 168 in layer 43). The sense wires for these dead channels were disconnected from their high voltage cables.

The loss of high voltage on a sense wire has an impact on the electrostatic field in surrounding cells, which will affect the drift behavior of ionized electrons and result in changes in drift lines and X - T relations. (In our case, cells 160 to 169 in layer 42 were affected.) The different charge distributions for normal cells and cells affected by dead channels are shown in Fig. 7, reflecting the change in the electric field and gas gain.

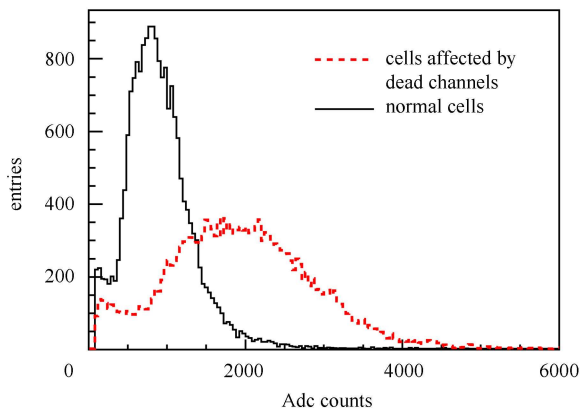


Fig. 7. Charge distributions for normal and dead channel cells.

The impact on the X - T relationship was studied using a Garfield [11] simulation. The difference in drift

distance between normal cells and cells affected by dead channels as a function of drift time is shown in Fig. 8. The difference is very small near the sense wire, but increases rapidly with drift time.

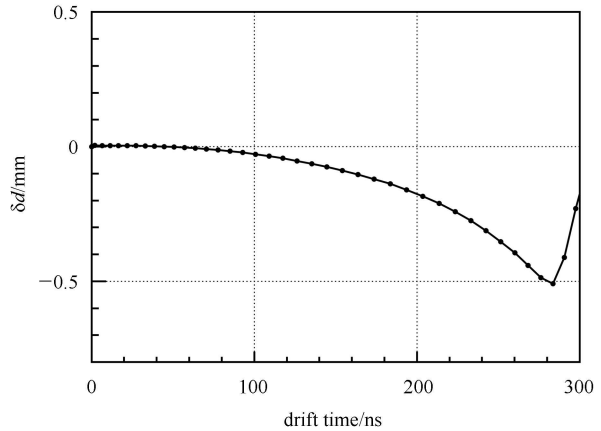


Fig. 8. The difference in X - T relations between normal cells and cells affected by dead channels, from Garfield simulation.

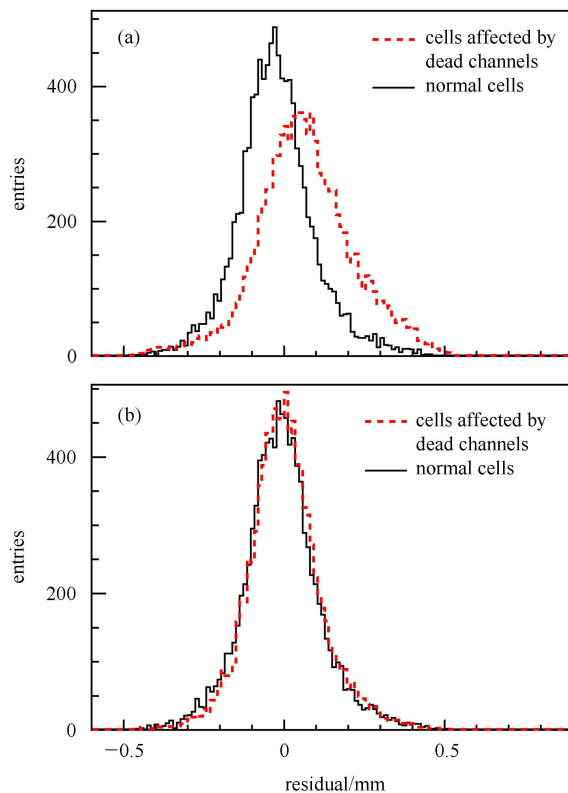


Fig. 9. Residual distribution for normal cells (solid line) and cells affected by dead channels (dashed line), (a) before recalibration and (b) after recalibration.

If we ignore the dead channels in the calibration, an incorrect X - T relationship will be obtained for those cells

affected by dead channels. This will cause bias in track fitting, which can produce an offset in the residual distribution, as shown in Fig. 9(a). This bias can cause a big difference in the reconstructed momentum for electrons and positrons that pass through the affected region ($\phi \approx 3.6$ rad), as shown in Fig. 10(a).

In order to minimize this bias, we calibrated the affected cells in layer 42 separately. The variation in the X - T relation obtained from the data is similar to the simulation result. The updated residual distributions are presented in Fig. 9(b), where the offset disappears. The difference in the reconstructed momentum for electrons and positrons in the affected region ($\phi \approx 3.6$ rad) is also reduced, as shown in Fig. 10(b). Similar results are obtained by using dimuon event samples. However, the reconstructed momentum is still not flat in the azimuth direction, which may be related to misalignment or some other reason—it is a subject of continuing studies.

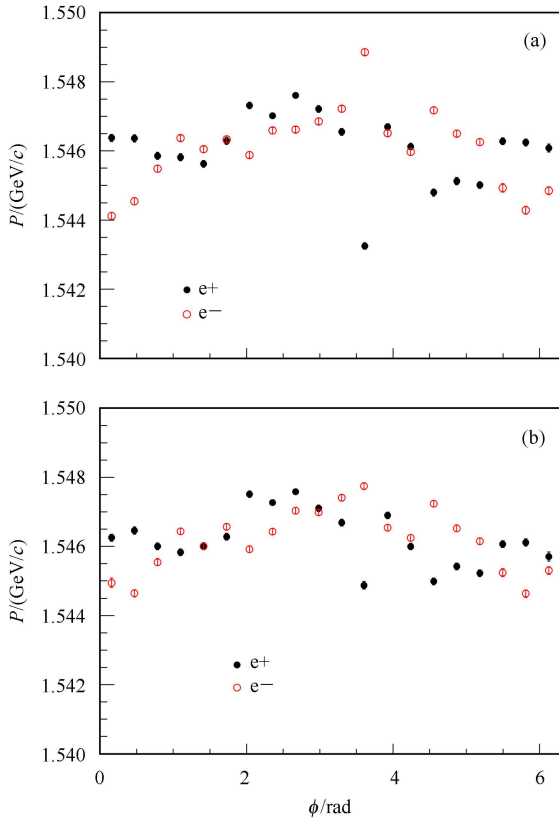


Fig. 10. The momentum as a function of ϕ for electron and positron ignoring (a) and considering (b) dead channels.

6 Momentum resolution and spatial resolution

After the complete calibration procedure is done, including the calibration of X - T relations, time offset, time

walk effects and alignment, the momentum and spatial resolutions are determined. Here, as an example, we report the result using the J/ψ data set collected in 2012. Fig. 11(a) shows the momentum distribution for

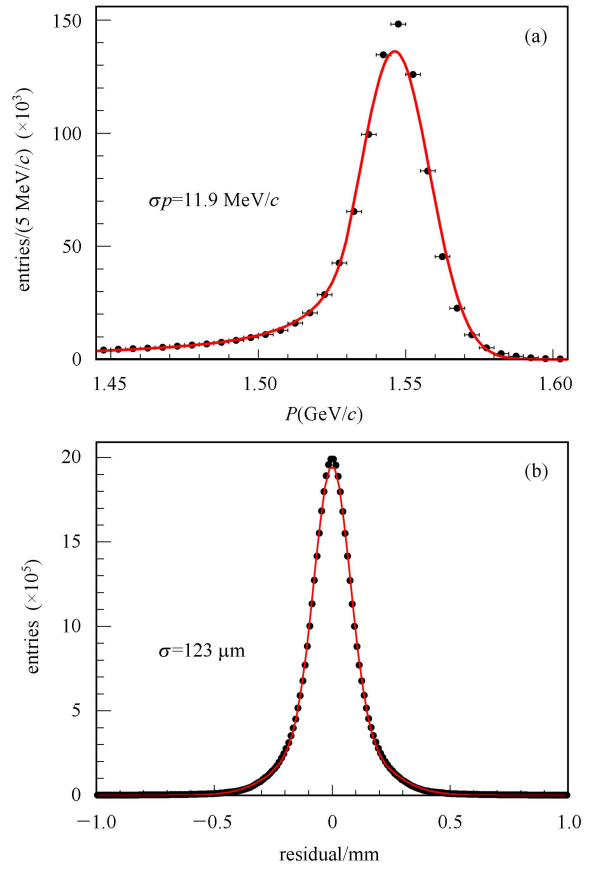


Fig. 11. Momentum resolution (a) and spatial resolution (b) for 1.548 GeV/c electrons from Bhabha events.

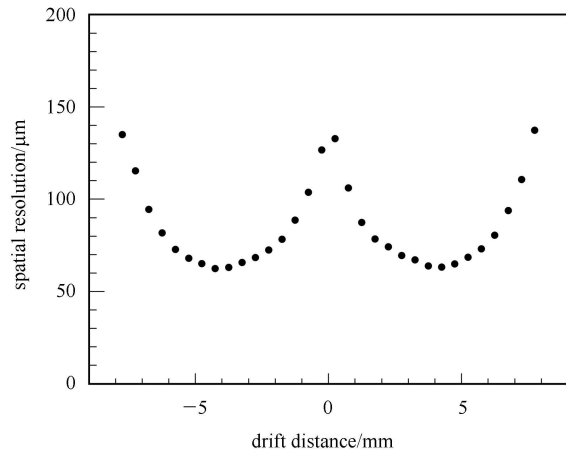


Fig. 12. Spatial resolution as a function of drift distance in layer 25.

1.548 GeV/ c electrons from Bhabha events. It is fitted with a Crystal Ball function and the momentum resolution is determined to be 11.9 MeV/ c . The spatial resolution, obtained from fitting a double Gaussian to the residual distribution, is 123 μm for Bhabha tracks averaged over the entire cells in all layers, as shown in Fig. 11(b). Fig. 12 shows the spatial resolution as a function of drift distance in layer 25. For tracks traversing the middle region between the sense and field wires, the spatial resolution is better than 65 μm , which is close to the intrinsic resolution of the chamber.

7 Summary

Our study is focused on the improvement of the calibration of the X - T relation for the BESIII drift chamber, as this has an important influence on track reconstruction. In the parameterization of the X - T relation, we adopt a numerical method. Taking into account the left-

right asymmetry due to the radial electric field asymmetry, different X - T relations are used for the left and right side of the sense wires. In order to improve the calibration of X - T relations with large entrance angles, we need to add low momentum data samples to the calibration procedure. The influence of dead channels is also studied. By re-calibrating the cells affected by adjacent dead channels, the residual deviation and the discrepancy between the reconstructed momentum for electrons and positrons in the ϕ direction are reduced effectively. By improving the calibration of X - T relations, shifts in track residuals are also reduced effectively. After all calibration procedures, the performance of the detector is obtained. Reconstruction of the Bhabha samples from the J/ψ data set collected in 2012 shows that the spatial resolution is 123 μm . In the middle region between the sense and field wire, the spatial resolution is better than 65 μm . The momentum resolution for 1.548 GeV/ c electrons is 11.9 MeV/ c .

References

- 1 Ablikim M et al. (BESIII collaboration). Nucl. Instrum. Methods A, 2010, **614**: 345–399
- 2 BEPCII Preliminary Design Report. 2002
- 3 LI W D, LIU H M et al. Proc. CHEP06. Mumbai 2006
- 4 WU Ling-Hui. Study of the Offline Calibration for the BESIII Drift Chamber and the Beam Test of a Prototype (PhD Thesis). Beijing: Institute of High Energy Physics, CAS, 2007 (in Chinese)
- 5 Belle Tracking Group. Charged Particle Tracking in Belle. Belle Note 327, 2000
- 6 Hirano H et al. (Belle collaboration). Nucl. Instrum. Methods A, 2000, **455**: 294–304
- 7 Ferrari A et al. (KLOE collaboration). Nucl. Instrum. Methods A, 2002, **494**: 163–172
- 8 WU L H, LIU J B et al. HEP & NP, 2005, **29**(05): 476–480 (in Chinese)
- 9 Peterson D et al. (CLEO III collaboration). Nucl. Instrum. Methods A, 2002, **478**: 142–146
- 10 WU L H, LIU J B et al. HEP & NP, 2006, **30**(07): 665–669 (in Chinese)
- 11 Veenhof R. Garfield help page: <http://garfield.web.cern.ch/garfield/help>